Simulation Modelling Practice and Theory 130 (2024) 102866

Contents lists available at ScienceDirect

Simulation Modelling Practice and Theory

journal homepage: www.elsevier.com/locate/simpat

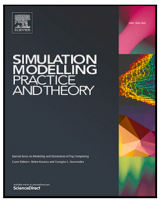

Modelling and simulation of interaction forces in tugboat-assisted docking of large marine vessels

Raymond Kristiansen [a,*], Henning Levik Ørke [b], Jan Tommy Gravdahl [b]

[a] UiT the Arctic University of Norway, Lodve Langesgate 2, Narvik, 8514, Norway
[b] Norwegian University of Science and Technology, O. S. Bragstadsplass 2D, Trondheim, 7491, Norway

ARTICLE INFO

Dataset link: https://github.com/raykris/Autodock

Keywords:
Marine vehicles
Tugboat-assisted docking
Interaction forces
Modelling and simulation

ABSTRACT

In this paper, we address modelling and simulation of dynamics involved in docking of large marine vessels with aid of tugboats, with the aim of providing a tool for improved design of control algorithms for autonomous docking operations. Mathematical models of the docking vessel and tugboats in 3DOF are derived, with a special focus on realistic interactions through towline, contact and friction forces with stick–slip dynamics and time delays, which are typically not considered in previous publications on the topic. We also present the implementation of the developed models in the first step towards a Simulink simulator in which considers the special case of tugboat-assisted docking operations in the Narvik harbour. The developed simulator is available on GitHub (see Ørke et al. (2023)) and encompasses model dynamics, tugboat control and vessel control and guidance, although the scope of this paper is model dynamics. We present simulation results that show that we are indeed able to capture interaction dynamics in a realistic way. Finally, we include a discussion of our results and some ideas for further development, as well as some concluding remarks.

1. Introduction

1.1. Background and motivation

Docking refers to the operation of manoeuvring a marine vessel safely to a dock in harbour for loading/unloading, and requires full knowledge of the vessels handling and propulsion system capabilities. The handling is determined from a vessel's pivot point, the point it rotates about, which changes depending on the forces that act on the vessel [1]. Large vessel's propulsion system usually consists of aft propellers and rudders that require forward velocity to turn, while some are equipped with bow tunnel thrusters to improve manoeuvring at lower velocities. Since the rudder use waterflow from the forward velocity to turn, the turning capability is reduced at low velocity and may cause loss of steering when propellers rotate astern when stopping. Astern moving propellers also cause more noticeable transverse thrust, which is a thrust force that causes the stern to move to either port or starboard from the interaction effects between propeller, rudder and hull. This effect can be used to bring the stern alongside the dock, but is hard to predict as the direction can change in shallow waters [2].

Harbours have velocity restrictions, dynamic traffic and limited area for manoeuvring, which makes docking operations challenging and must be carefully planned out with high enough velocity to steer the vessel, but low enough to be able to stop. In addition, wind and ocean currents would also affect the manoeuvring and increase the difficulty of the docking operation. While the forces have larger impact on the alongside of the vessel, the current direction close to the dock can create problems. A current

* Corresponding author.
E-mail addresses: raymond.kristiansen@uit.no (R. Kristiansen), henning.orke@gmail.com (H.L. Ørke), jan.tommy.gravdahl@ntnu.no (J.T. Gravdahl).

https://doi.org/10.1016/j.simpat.2023.102866
Received 6 July 2023; Received in revised form 1 November 2023; Accepted 20 November 2023
Available online 22 November 2023

that moves with the vessel would require astern motion to stop, while docking against the current could push the vessel towards or away from the dock, depending on the incident angle with the dock. When approaching the dock, the restricted waterflow between the vessel and dock can cause interactive forces that can pull the ship towards the dock or push it away. Due to these challenges, tugboat-assisted docking is often necessary or required [2].

Tugboat-assisted docking operations often require multiple tugboats that are strategically placed around the hull of the towed vessel, where they can apply pushing or pulling forces. The effectiveness of the tug will depend on the position from the pivot point. For a ship moving forward, the pivot point would move ahead, where a tugboat placed closer to the stern would have more effect in rotating the ship than a tugboat closer to the bow [2]. For most cases, tugboat operations are coordinated through radio communication by an experienced pilot of the harbour onboard the towed vessel, and skilled helmsmen that manually operate the tugboats. As each operation is unique, due to winds, ocean currents and dynamic traffic in ports, the pilot must adjust the towing operation along the way. Ships that require assistance are usually massive in both size and weight, where every action must be planned and carefully carried out. By automating the operation, the collaboration between the tugboats can be significantly improved. This will require solutions through advanced nonlinear control theory combined with optimisation problems, to compute the necessary forces and positioning of each tugboat. Manual coordination through radio communication can thus be relaxed, resulting in improved efficiency, time, and safety.

1.2. Relevant studies

Several studies on manoeuvring surface vessels by considering multiple tugboats as hull-attached "thrusters" have been performed. Control solutions usually consists of four to six tugboats, opposite paired around the hull, where they can apply pushing forces with limited rotational capabilities. Esposito et al. [3] developed a force allocation strategy together with adaptive control to compensate for unknown hydrodynamic parameters, achieving asymptotically convergent reference tracking with six tugboats as thrusters. The thrust allocation is solved as a least square optimisation problem with linear constraints, and is validated through model scale testing. With a similar approach, Bui et al. [4] solves the control allocation as an optimisation problem, by using the redistributed pseudo-inverse to find desirable directional thrust force for the tugboats. The study uses four tugboats on an unactuated vessel, with limited pushing force and directional change, and manage to follow a path with desired velocities in Matlab simulations. An adaptive controller is also implemented to account for the uncertainty in draft coefficients of the damping matrix. By using the same method to solve the control allocation problem, Bui et al. [5] shows that a sliding mode controller can be used for slow speed trajectory tracking, which have desirable performance in the presence of environmental disturbances. The controller is simulated with a small model, where a nonlinear observer is used to estimate position from noisy measurements. In [6], a floating structure is manoeuvred with three autonomous surface vehicles (ASV) in a triangular formation, by combining pushing force at the stern and towline forces on each side. The towline forces are modelled with nonlinear dynamics, where the tugboats are attached to the floating structure with two towlines each, one to aft and the other to fore, to allow for surge, sway and yaw control. Simulation results show that a predefined trajectory can be followed, with both static and dynamic obstacles, by using model-predictive control to control the ASVs and alternating direction methods for consensus. A related control problem is also found in dynamic positioning (DP) systems, which are used to keep overactuated marine vessels in a desired position and heading by using their own propulsion systems *-cf.* [7,8]. For a more comprehensive review, we refer interested readers to Du et al. [9] and references therein.

As shown above, several studies have focused on tugboat-assisted docking operations to manoeuvre a large ship or structure, with control approaches capable of handling model parameter uncertainties, environmental disturbances and obstacle avoidance. The common practice among the prior studies is however that tugboats are usually placed on both sides of the towed object and in fixed position to immediately give the desired forces. Since tugboat-assisted docking operations are carried out from one side of the towed object, the tugboats would require repositioning to change the force direction. This will cause a significant time delay when switching between pushing and pulling, which leaves the docking vessel partially uncontrolled for a certain time span. Moreover, previous studies usually have assumptions of no slip along the hull as well as fixed tugboat incident angles on the hull, which simplifies the control design significantly, but is not realistic in real operations and also reduces the control flexibility.

To support the development of control algorithms for tugboat-assisted docking of vessels, this paper presents the first step in developing a simulator for a realistic implementation of dynamic forces and moments on vessels and tugboats during docking operations, with a special focus on interaction forces as well as the time delay required to move tugboats in positions to give either pushing or pulling forces [10]. The work is based on tugboat operations in Narvik harbour (Fig. 1), where large quantities of iron ore are shipped out with bulk carriers, with length of 200–300 m, width 30–45 m, and carrying capacity between 60 000 to 180 000 tonne. There are three tugboats stationed in Narvik: Bulldog, Barents and Rombak.[1] These tugboats have either azimuth or voith propulsion systems capable of producing thrust in 360°. The bulk carriers are docked with starboard side when loading ore to reduce manoeuvring when leaving the harbour fully loaded, and three tugboats are used on the port side (Fig. 1) for the docking operation.

In our paper, we present the theoretical derivations for the simulator of a bulk carrier and supporting tugboats, with interaction forces between them to simulate towline forces and contact forces with stick–slip dynamics. At this stage, the simulator assumes 3DOF operations of marine crafts, ideal weather conditions with no ocean currents, wind or waves, and that thrust forces have no correlating effect that reduces efficiency.

[1] See Buksér og Berging: https://www.bube.no/our-vessels/.

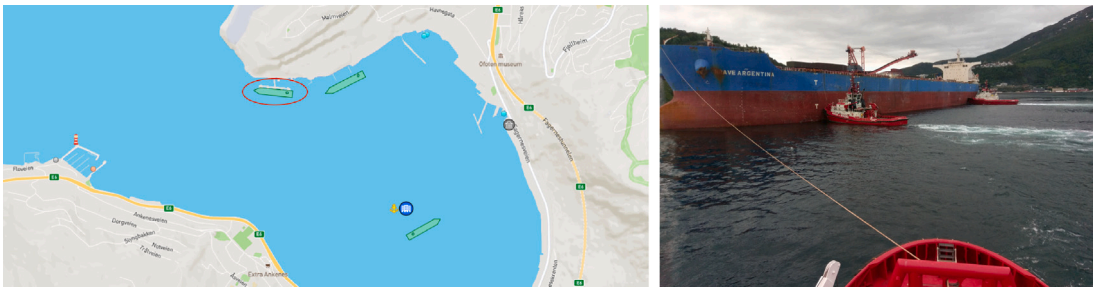

Fig. 1. Left: Narvik harbour, the red circle shows a bulk carrier loading ore at the dock. Image taken from live map at Marinetraffic.com on 16. November 2021. Right: Manual tugboat-assisted docking of a bulk carrier in Narvik (*Photo: R. Kristiansen*).

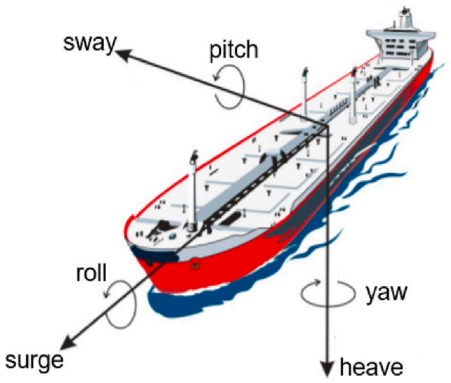

Fig. 2. The body fixed linear velocities (surge, sway, heave) and angular velocities (roll, pitch, yaw) for a surface vessel. *Source:* Edited from [1].

1.3. Outline

Section 2 presents the theoretical background for developing a mathematical model for a surface vessel with supporting tugboats in 3DOF. Section 3 presents the method of implementing the bulk carrier and tugboat dynamics and the interaction forces between them, while simulation results and discussion of the model and interaction forces are given in Section 4. Finally, we conclude the paper in Section 5, and recommend some improvements for further work.

2. Mathematical modelling

This section presents the theory used to develop the mathematical model of the vessel dynamics and interaction forces. Unless otherwise noted, derivations are based on [1].

2.1. Marine craft dynamics

The motion of a marine craft can be described by six body-fixed linear and angular velocities, as shown in Fig. 2. By assuming that the rotation in roll and pitch are small, these can be neglected for surface vessels and simplifies the motion of a marine craft to 3DOF and allows representing the dynamics two dimensions with surge, sway and yaw.

2.1.1. Kinematics

The kinematics of a marine craft are represented in two reference frames, where the first is used to describe the position and orientation, while the second describes linear and angular velocities. For geographical areas of less than 10×10 km^2, position and orientation of a marine craft can be represented accurately in the NED reference frame, denoted $\mathcal{F}_n$, which spans a tangential plane with origin located at the Earth's reference ellipsoid, with axes $[x_n, y_n, z_n]$ pointing respectively to true north, east, and the Earth's centre. Linear and angular velocities are represented in the body reference frame $\mathcal{F}_b$ fixed to the marine craft. The frame origin is at the waterline in the centre of the vessel, with axes $[x_b, y_b, z_b]$ pointing respectively towards the bow, starboard and keel.

Position and orientation of the marine craft are described by the $\mathcal{F}_b$ relative to $\mathcal{F}_n$ (see Fig. 3). Position is represented by the coordinates $[x^n, y^n]$ of the $\mathcal{F}_b$ origin in $\mathcal{F}_n$. Orientation is given by the angle between true north x_n and the bow direction x_b, which is

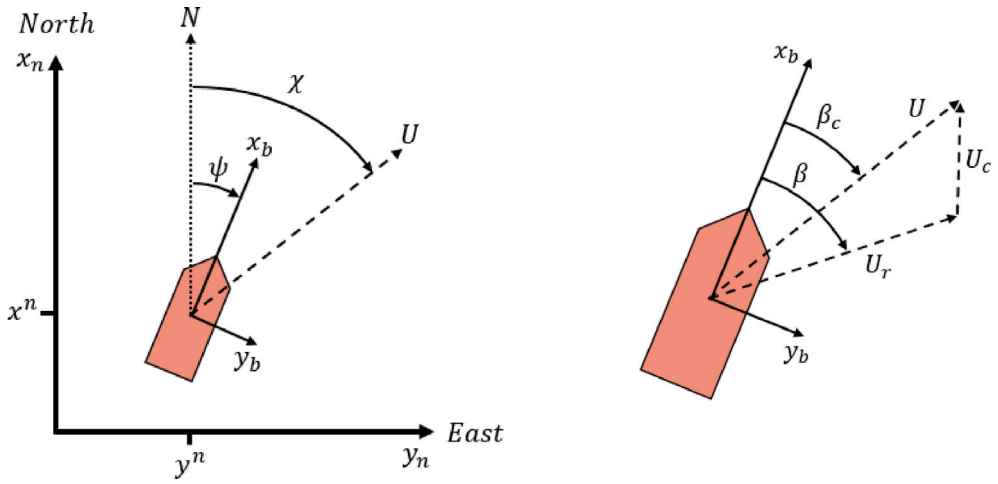

Fig. 3. Left: Body reference frame $\mathcal{F}_b$ in NED $\mathcal{F}_n$ related by the coordinates $[x^n, y^n]$ and heading angle ψ, with course angle χ. Right: Surface velocity U composed of relative velocity U_r and ocean current U_c, with crab angle β_c and sideslip β.
Source: Edited from [1].

referred to as heading ψ and is clockwise positive. While heading describes the orientation of the marine craft, the linear movement is represented by the course over ground χ as

$$\chi = \psi + \beta_c \,. \tag{1}$$

Here, β_c is the crab angle, which is the angle of the speed over ground U of the marine craft in $\mathcal{F}_b$ (see Fig. 3). The surface velocity is composed of the linear velocity in surge u and sway v, which consist of the ocean current and relative velocity, such that

$$U = U_c + U_r \rightarrow \begin{bmatrix} u \\ v \end{bmatrix} = \begin{bmatrix} u_c + u_r \\ v_c + v_r \end{bmatrix} . \tag{2}$$

In the absence of ocean currents, the crab angle is equal to the sideslip β, which is caused by the relative velocity of the marine craft. The kinematics of the marine craft are given by the position and orientation vector $\boldsymbol{\eta}$ and linear and angular velocity vector $\boldsymbol{\nu}$ as

$$\boldsymbol{\eta} = \begin{bmatrix} x^n & y^n & \psi \end{bmatrix}^\top , \qquad \boldsymbol{\nu} = \begin{bmatrix} u & v & r \end{bmatrix}^\top \tag{3}$$

where r is the angular velocity in yaw/heading. The linear and angular velocities $\boldsymbol{\nu}$ can further be used to find the change in position and orientation $\boldsymbol{\eta}$ with

$$\dot{\boldsymbol{\eta}} = \boldsymbol{R}_b^n(\psi)\boldsymbol{\nu} \tag{4}$$

where $\boldsymbol{R}_b^n(\psi) \in SO(3) = \{\boldsymbol{R} | \boldsymbol{R} \in \mathbb{R}^{3\times3}, \boldsymbol{R}^\top \boldsymbol{R} = \mathbf{I}, \det \boldsymbol{R} = 1\}$ is the rotation matrix from $\mathcal{F}_b$ to $\mathcal{F}_n$ given by (*cf.* [11])

$$\boldsymbol{R}_b^n(\psi) = \begin{bmatrix} \cos(\psi) & -\sin(\psi) & 0 \\ \sin(\psi) & \cos(\psi) & 0 \\ 0 & 0 & 1 \end{bmatrix} . \tag{5}$$

2.1.2. Kinetics

Kinetics describe the translational and rotational motion of a marine craft, derived by using vectorial mechanics and the Newton–Euler formulation, and given by

$$\boldsymbol{M}_{RB}\dot{\boldsymbol{\nu}} + \boldsymbol{C}_{RB}(\boldsymbol{\nu})\boldsymbol{\nu} = \boldsymbol{\tau}_{RB} \tag{6}$$

where $\boldsymbol{M}_{RB}$ is the rigid-body mass matrix, $\boldsymbol{C}_{RB}(\boldsymbol{\nu})$ represents the Coriolis and centripetal forces caused by the rotation between reference frames, while $\boldsymbol{\tau}_{RB} = [X, Y, N]^\top$ are the external forces and moments in $\mathcal{F}_b$. The equations of motion may either be represented in the centre of gravity (CG) or in the coordinate origin (CO), where the latter is the origin of $\mathcal{F}_b$. CG is located at a distance from CO, given by the vector $\boldsymbol{r}_{bg}^b = [x_g, y_g, z_g]^\top$. In our work, we represent our equations of motion in CO, to match computations of hydrodynamic forces and moments [1].

2.1.3. Hydrodynamic forces

Surface vessels float when they displace a volume of water equal to their mass. For the vessel to move, the water has to move around the hull to give space for the vessel and replace the previous displaced volume. This creates hydrodynamic forces on the

hull, which can be included by expanding (6) with added virtual mass and damping, giving manoeuvring equations of motion as

$$\underbrace{\boldsymbol{M}_{RB}\dot{\boldsymbol{\nu}} + \boldsymbol{C}_{RB}(\boldsymbol{\nu})\boldsymbol{\nu}}_{\text{rigid-body forces}} + \underbrace{\boldsymbol{M}_{A}\dot{\boldsymbol{\nu}}_r + \boldsymbol{C}_{A}(\boldsymbol{\nu}_r)\boldsymbol{\nu}_r + \boldsymbol{D}(\boldsymbol{\nu}_r)\boldsymbol{\nu}_r}_{\text{hydrodynamic forces}} = \boldsymbol{\tau}\,. \tag{7}$$

The hydrodynamic forces consist of damping $\boldsymbol{D}(\boldsymbol{\nu}_r)$, added mass for the inertial matrix $\boldsymbol{M}_A = [A_{ij}]$ and Coriolis and centripetal forces $\boldsymbol{C}_A(\boldsymbol{\nu}_r)$. The hydrodynamic forces depend on the relative velocity $\boldsymbol{\nu}_r$, which includes the irrotational ocean currents $\boldsymbol{\nu}_c$.

Linear damping. The damping $\boldsymbol{D}(\boldsymbol{\nu}_r)$ can be divided into linear damping $\boldsymbol{D}$ consisting of potential damping and skin friction, and quadratic damping $\boldsymbol{D}_n(\boldsymbol{\nu}_r)$;

$$\boldsymbol{D}(\boldsymbol{\nu}_r) = \boldsymbol{D} + \boldsymbol{D}_n(\boldsymbol{\nu}_r)\,. \tag{8}$$

Linear damping causes the velocity to exponentially decay to zero and is important for station keeping and low speed manoeuvring, while quadratic damping dominates at higher velocities [1]. In manoeuvring models the closed-loop natural periods for stabilising surge, sway and yaw motion are between 0.03–0.10 rad/s, and due to the low frequency, added mass and potential damping can be approximated at zero wave excitation frequency, where the potential damping is zero and the linear damping is dominated by the viscous damping. The viscous damping can be chosen as

$$\boldsymbol{B}_V(\omega) = \operatorname{diag}\left\{\beta_1 e^{-a\omega} + N_{\text{ITTC}}(A_1), \beta_2 e^{-a\omega}, \beta_6 e^{-a\omega}\right\} \tag{9}$$

with exponential rate $a > 0$, wave excitation ω, linear surge resistance $N_{\text{ITTC}}(A_1)$ and the linear viscous skin friction coefficients $\beta_{1,2,6}$ [1]. The skin friction coefficients for surge, sway and yaw can be found from the three mass–damper systems

$$\beta_{v_1} = \frac{m + A_{11}(0)}{T_1}, \qquad \beta_{v_2} = \frac{m + A_{22}(0)}{T_2}, \qquad \beta_{v_6} = \frac{I_z + A_{66}(0)}{T_6} \tag{10}$$

with time constants $T_{1,2,6}$, mass of the marine craft m, the diagonal elements of the added mass matrix $A_{1,2,6}$ and inertia in yaw I_z.

Nonlinear damping. The nonlinear surge damping can be modelled as

$$X = -\frac{1}{2}\rho S(1+k)C_f(u_r)|u_r|u_r \tag{11a}$$

$$C_f(u_r) = \frac{0.075}{(log_{10}(R_n) - 2)^2 + \epsilon} + C_R \tag{11b}$$

$$R_n = \frac{L_{pp}}{\nu_v}|u_r| \geq 0 \tag{11c}$$

where the damping force X depends on the relative surge velocity u_r, with density ρ, wetted hull surface S, viscous correction factor k and the friction coefficient C_f. Typical values of the viscous correction factor are $k = 0.1$ for ship in transit and $k = 0.25$ for DP operations, while a tanker have around $k = 0.3$ [1]. The friction coefficient C_f depends on the residual friction C_R, a small number ϵ to keep it well defined, and Reynolds number R_n, which are calculated based on the length between perpendiculars[2] L_{pp} and the kinematic viscosity ν_v.

The nonlinear damping in sway and yaw can be calculated from the cross-flow drag principle. Cross-flow drag is difficult to calculate due to velocity in surge. For very low surge velocities, the effect is less prominent and can be neglected when calculating the transverse movement. The sway force Y and yaw moment N can be found by using a strip theory approach as

$$Y = -\frac{1}{2}\rho \int_{-\frac{L_{pp}}{2}}^{\frac{L_{pp}}{2}} T(x)D_d^{2D}(x)|v_r + xr|(v_r + xr)dx \tag{12}$$

$$N = -\frac{1}{2}\rho \int_{-\frac{L_{pp}}{2}}^{\frac{L_{pp}}{2}} T(x)D_d^{2D}(x)x|v_r + xr|(v_r + xr)dx \tag{13}$$

depending on the relative sway velocity v_r, yaw rate r, length between perpendiculars L_{pp}, density ρ, 2D drag coefficient $C_d^{2D}(x)$ and draft $T(x)$, which are calculated at the longitudinal distance x.

2.1.4. Thrust force and moments

Forces and moments for marine crafts are created by effectors and actuators. Effectors are mechanical devices that create time-varying mechanical forces and moments, such as propellers and rudders, while actuators control the magnitude and direction of the effectors with electromechanical devices [12]. For a fixed pitch propeller, thrust force and torque can generally be calculated from

$$\text{Thrust} = \rho D^4 K_T(J_a)|n_p|n_p \tag{14}$$

$$\text{Torque} = \rho D^5 K_Q(J_a)|n_p|n_p \tag{15}$$

[2] The length of the vessel along the waterline from the forward surface of the stem to the after surface of the sternpost.

with density ρ, propeller diameter D, propeller revolution per second n_p and propeller coefficients for thrust K_T and torque K_Q. The coefficients K_T and K_Q depends on the open-water advanced coefficient J_a, which adjust the performance of the propeller depending on the forward velocity u and a wake fraction number w according to

$$J_a = \frac{u_a}{n_p D}, \qquad u_a = (1 - w)u\,. \tag{16}$$

The forces and moments from effectors on the marine craft can be computed by summing up the thrust contribution into the DOF they affect. This gives the vector $\boldsymbol{\tau}$ of forces and moments located at the $\mathcal{F}_b$ origin CO, which includes the surge and sway forces F_x and F_y from the thrusters location in the body reference frame $[l_x, l_y]$, such as

$$\boldsymbol{\tau} = \sum_{i=1}^{r} \begin{bmatrix} F_{x_i} \\ F_{y_i} \\ F_{y_i} l_{x_i} - F_{x_i} l_{y_i} \end{bmatrix}. \tag{17}$$

The force and moment vector $\boldsymbol{\tau} \in \mathbb{R}^3$ can be calculated from the input vector $\boldsymbol{u} \in \mathbb{R}^r$ with

$$\boldsymbol{\tau} = \boldsymbol{B}\boldsymbol{u} = \boldsymbol{T}\boldsymbol{K}\boldsymbol{u} \tag{18}$$

where r is the number of effectors. In the equation, $\boldsymbol{B} \in \mathbb{R}^{3\times r}$ is the input matrix that can be divided into a thrust coefficient matrix $\boldsymbol{T} \in \mathbb{R}^{3\times r}$ and force coefficient matrix $\boldsymbol{K} \in \mathbb{R}^{r\times r}$. Depending on the number of DOF and effectors, the system is either fully actuated ($r = 3$), underactuated ($r < 3$) or overactuated ($r > 3$). The number of effectors is increased by using azimuth thrusters that can rotate 360°, which results in a force that can contribute in both surge $F_x = \cos(\alpha)F$ and sway $F_y = \sin(\alpha)F$. The forces depend on the angle of attack α, represented in $\mathcal{F}_b$, which is clockwise positive from the marine crafts heading.

2.2. Interaction forces

Interaction between the towed vessel and tugboats is performed by either a pulling or a pushing operation. Pulling requires the use of towlines of a certain length, which when stretched out will provide a towline force on the vessel. To provide a realistic simulation of towline force, we take into account towline elasticity and stiffness, which will result in a dynamic application of force during the pulling operation. This is especially noticeable in the transient when the towline reaches the fully stretched state, and dampens out when the pushing force is steadily applied. Other factors are the vertical angle of the towline and propeller wash deflected from the vessel hull when the distance between the tugboat and vessel is small, but these are not implemented in the simulator at this stage. Pushing is performed by direct contact between the vessel and tugboat, producing a contact force that allows moving the vessel in its lateral direction. The contact force may be further split into a normal force perpendicular to the hull (providing the push) as well as a friction force tangential to the hull (preventing sliding of tugboats along the vessel hull). Thus, changing between pulling and pushing forces requires relocation of the tugboat which further causes delays in application of forces. Important dynamics for providing a realistic contact force simulations is mainly related to the tugboat and vessel surfaces. We assume that the vessel hull is steel, and that the tugboat has a rubber fender that may be compressed, which can be modelled as a mass–spring–damper system. Similar to the towline force, this dynamic will be most noticeable in the transition when the tugboat approaches the vessel, but dampens out when constant pressure is applied.

2.2.1. Towline force

In towing operations, the towline is attached to pullerts at deck level on the towed structure. For bulk carriers, the towing point is above the tugboat, which can make a significant vertical angle on the towline. The pulling force is not affected by the angle and is equal to the thrust force, but results in a vertical force that lift the tugboat and increases the towline tension. The increased tension cause higher friction forces in the fairleads, which increase the risk of breaking the towline [13]. A longer towline can reduce the tension, but harbours have restricted space for manoeuvring, which limits the length of the towline. While a shorter towline has faster response time to change tugboat position, it shortens the distance between the tugboat thrust force and the towed vessel. The interacting propeller wash from the thrust force can then deflect on the hull and disturb the water surrounding the thrusters, as shown in Fig. 4. This effect opposes the thrust force and can cause cavitation with increased effect for shorter towlines [14].

The interacting propeller wash should be accounted for with short towlines, where the required bollard pull can be estimated from an interacting efficiency factor a_{int} as [15]

$$a_{\text{int}} = \left[1 + 0.015 A_{\text{exp}}/L_{\text{t}}\right]^{-h} \qquad L_{\text{t}} > 30 \text{ [m]} \tag{19}$$

where A_{exp} is the projected area on the towed vessel, L_{t} is the towline length and h is a factor depending on the towed shape, with $h = 1.6$ for ship-shaped objects and $h = 2.1$ for barges [15]. If the towed structure is much larger relative to the tugboat propeller, the waterflow can result in a negative effect larger than the thrust force, giving motion in the opposite direction [16].

Thrust force close to the bow or stern of the towed vessel can also reduce the tow efficiency due to the Coanda effect, which is the tendency for a fluid stream to follow a convex surface instead of going in the initial direction (*cf.* [17]). This effect can create a negative pressure on the opposing side, which can counteract the towing force and even cancel it out, where increasing the pulling force would increase the waterflow and the effect [14].

The stiffness of a towline consists of two parts, elastic elongation k_E and change in the catenary geometry k_G [16]. Catenary gives a curvature of the towline depending on the weight, while the elongation depends on the material type. When the towline

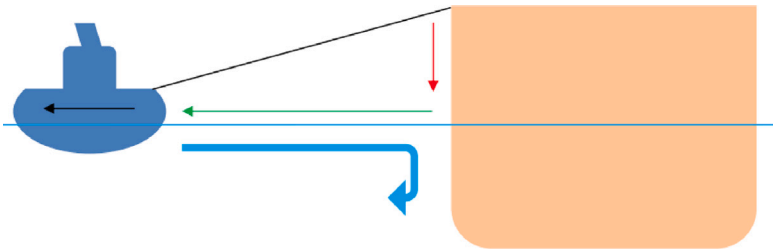

Fig. 4. Illustration of propeller wash [14].

tension is high, the stiffness due to elastic elongation k_E dominates and can be used to approximate the total stiffness k of the towline, such that [16]

$$k = \frac{k_G k_E}{k_G + k_E} \qquad k_E = \frac{EA}{L_t} \qquad k_G = \frac{12T_0^3}{(wL_t)^2 L_t} \tag{20}$$

with towline tension T_0, submerged weight per towline length w, towline length L_t and nominal cross section area A, while E is Young's modulus of elasticity. The combined stiffness k is only valid for slowly changing motion, with periods over 30 s [16].

2.2.2. Contact force

The pushing force from tugboats are limited to certain strong sections on the side of the vessel [14], and when the tugboats are pushing, the contact force compresses the tugboat's rubber fender. The resulting force consist of a normal force perpendicular to the hull, and a friction force tangential to the hull.

Normal force. By using a dissipative contact force model, seen as a linear spring in parallel with a linear damper, the normal force can be computed from [18]

$$F_N = K\delta + D\dot{\delta} \tag{21}$$

where K is the stiffness parameter related to the elastic force, D is the damping coefficient for the dissipative force and δ is the relative distance of deformation. The equation causes unrealistic behaviour when the damping force contributes while the deformation is zero, $\delta = 0$ and $\dot{\delta} \neq 0$. For higher material damping, the viscoelastic nature can be represented with a damping factor based on the product of elastic force and velocity [18].

Friction force. Friction reduces or prevents the tugboats from sliding along the hull of the towed vessel. The friction force F_R can be calculated from the Coulomb friction model for a general velocity v as

$$F_R = \mu F_N \operatorname{sgn}(v), \qquad v \neq 0 \tag{22}$$

which however is not defined for zero velocity between the contacting surfaces. Coulomb friction is a static friction model that opposes movement along a surface with a force that is proportional to the normal force F_N, based on the friction coefficient μ [11]. The friction coefficient is a dimensionless number that depends on the material of the contacting surfaces and lubrication between them. In some static friction models, the friction is larger at zero velocity than under sliding. This can be modelled with a static friction coefficient μ_s when there is no motion and a kinetic friction coefficient μ_k when there is sliding motion -*cf.* [19]. The change in coefficient gives a discontinuous stick–slip motion, where the contacting surfaces sticks together when the velocity is zero and the force is lower than the static friction force, and starts to slide when the static friction force is exceeded [11].

3. Model implementation

The simulator model (see [10]) was developed in Simulink with Matlab version R2023a, by using the MSS toolbox [20]. The model is divided into three categories, model dynamics, tugboat control system and bulk carrier control and guidance systems. In the following, the implementation method for the model dynamics is described. This section explains the mathematical models for the bulk carrier and tugboat dynamics, and the interaction forces caused by direct contact and from the towline (see Fig. 5).

3.1. Implementing vessel dynamics

3.1.1. Bulk carrier dynamics

To simulate the dynamics of a bulk carrier, the dynamics are based on data from a Wamit file of a tanker, obtainable from the MSS toolbox [20]. Wamit is a computer program that solves 3D potential theory by dividing the hull in contact with water into elements. This method is suitable for offshore applications at zero-forward velocity and can be used to find frequency-dependent added mass and potential damping [1]. The specification of the Tanker is given in Table 1.

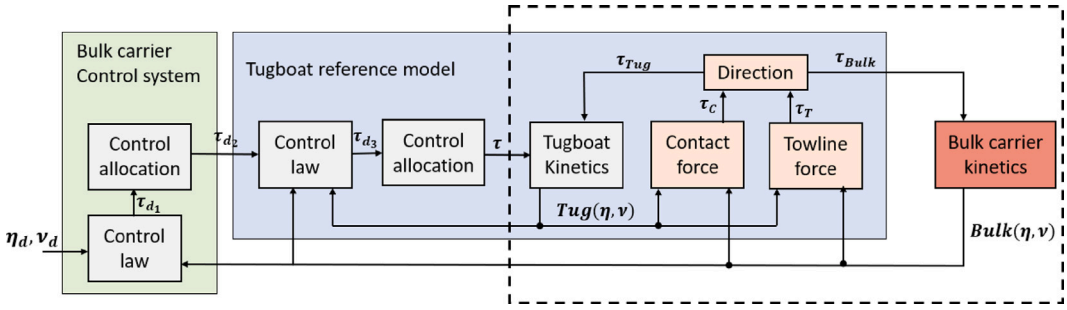

Fig. 5. Illustration of the vessel kinetics and interaction forces in the Simulink model covered in Section 3, within the dotted line.

Table 1
Specification of the Wamit files, Tanker and FPSO, from the MSS toolbox [20]. Length is given as the length between the perpendiculars.

Vessel	Length	Width	Draft	Weight
Tanker	246 m	46 m	10 m	94 620 t
FPSO	200 m	46 m	10 m	100 410 t

The rigid body mass matrix $\boldsymbol{M}_{RB}$ and Coriolis and centripetal matrix $\boldsymbol{C}_{RB}(\boldsymbol{\nu})$, represented in CO with $\boldsymbol{r}_{bg}^{b} = [3.9, 0]^{\top}$, were found with the function "rbody" from the MSS toolbox. To convert the matrices into 3DOF the effect from heave, roll and pitch were neglected, such that

$$\boldsymbol{M}_{RB} = \begin{bmatrix} m & 0 & 0 \\ 0 & m & mx_g \\ 0 & mx_g & I_z \end{bmatrix} \quad \boldsymbol{C}_{RB}(\boldsymbol{\nu}) = \begin{bmatrix} 0 & -mr & -mx_g r \\ mr & 0 & 0 \\ mx_g r & 0 & 0 \end{bmatrix}. \tag{23}$$

Both the rigid body added mass matrix $\boldsymbol{M}_A$ and the potential damping matrix $\boldsymbol{D}_p$ was found at zero wave excitation frequency (ie. $\omega = 0$), while the added mass Coriolis and centripetal matrix $\boldsymbol{C}_A(\boldsymbol{\nu}_r)$ was computed from $\boldsymbol{M}_A$ with the function "m2c" from the MSS toolbox. The matrices used are shown in (24), and since we assume ideal conditions with no ocean currents, $\boldsymbol{\nu}_r = \boldsymbol{\nu}$.

$$\begin{aligned} \boldsymbol{M}_A &= -\begin{bmatrix} X_{\dot{u}} & 0 & 0 \\ 0 & Y_{\dot{v}} & Y_{\dot{r}} \\ 0 & N_{\dot{v}} & N_{\dot{r}} \end{bmatrix} = \begin{bmatrix} A_{11}(0) & 0 & 0 \\ 0 & A_{22}(0) & A_{26}(0) \\ 0 & A_{62}(0) & A_{66}(0) \end{bmatrix} \\ \boldsymbol{C}_A(\boldsymbol{\nu}_r) &= \begin{bmatrix} 0 & 0 & Y_{\dot{v}} v_r + Y_{\dot{r}} r \\ 0 & 0 & -X_{\dot{u}} u_r \\ -Y_{\dot{v}} v_r - Y_{\dot{r}} r & X_{\dot{u}} u_r & 0 \end{bmatrix} \\ \boldsymbol{D}_p &= 0. \end{aligned} \tag{24}$$

There is no potential damping at zero wave excitation, and thus the linear damping only consists of viscous damping $\boldsymbol{D}_v$. The viscous damping given in the tanker Wamit file needed adjustments and was instead calculated from (9) with time constants of a mass–damper system. As the FPSO has relatively similar proportions as the tanker file (see Table 1), the time constants of the FPSO, given as $T_1 = 100$, $T_2 = 17$ and $T_6 = 18$ were used as starting point. First the time constant T_1 was increased, since the FPSO is built for standing still on DP and has a relatively flat front area compared to the tanker. While the tanker is longer, the FPSO has flatter surfaces and thus increased resistance for moving in water. The constants T_2 and T_6 were therefore set similarly to the FPSO. Thus, we obtain a diagonal damping matrix

$$\boldsymbol{D} = -\begin{bmatrix} X_u & 0 & 0 \\ 0 & Y_v & 0 \\ 0 & 0 & N_r \end{bmatrix} = \begin{bmatrix} \beta_{v_1} & 0 & 0 \\ 0 & \beta_{v_2} & 0 \\ 0 & 0 & \beta_{v_6} \end{bmatrix} \tag{25}$$

computed with the time constants $T_1 = 160$, $T_2 = 19$ and $T_6 = 21$. The surge resistance term $A_{\mathrm{ITTC}}(A_1)$ was neglected since it is a linearisation of the quadratic damping in surge, which is small due to low velocity.

3.1.2. Tugboat dynamics

The simulated tugboat was based on Bulldog from the company "Buksér og Berging AS," which is stationed in Narvik. Bulldog is an azimuth stern drive (ASD) tug that is equipped with two azimuth thrusters for main propulsion, and a tunnel thruster at the bow to increase manoeuvrability at low velocities. The effectiveness of the tunnel thrusters can be lost between 1–2.5 m/s [2]. ASD tugs have towline connection at the bow and are equipped with rubber fenders around the bow, as seen in Fig. 6. The tugboat model was implemented by using the 3DOF manoeuvring model given in (7), with nonlinear damping $\boldsymbol{d}(\boldsymbol{\nu})$, such that

$$\boldsymbol{M}\dot{\boldsymbol{\nu}} + (\boldsymbol{C} + \boldsymbol{D})\boldsymbol{\nu} + \boldsymbol{d}(\boldsymbol{\nu}) = \boldsymbol{\tau} \tag{26}$$

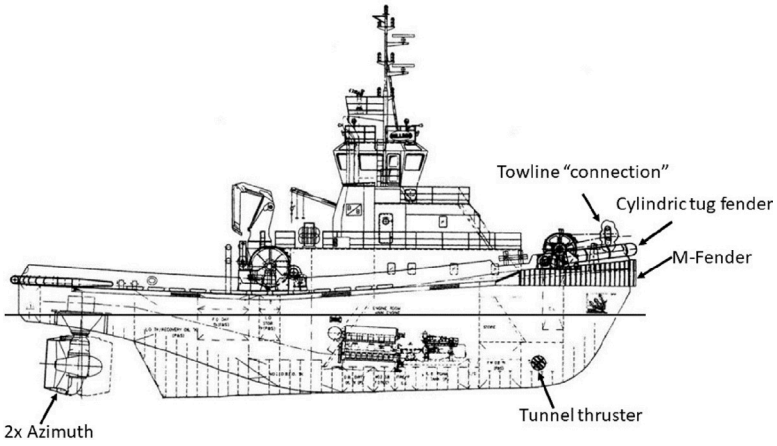

Fig. 6. Illustration of BB Bulldog.
Source: Edited from [21].

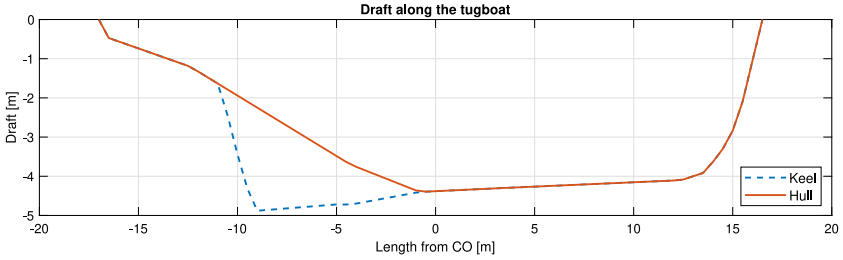

Fig. 7. Draft along the tugboat based on the illustration in Fig. 6.

Table 2
Data on vessels used to implement the model of BB Bulldog. Navel vessel from the MSS toolbox [20], and a similar tugboat model used for escort operations with full scale from Piaggio et al. [22]. Length is given as the length between the perpendiculars.

Vessel	Length	Width	Draft	Displacement	Wet surface
Naval	51.5 m	8.6 m	2.3 m	362 m^3	–
Tug model	27.5 m	12 m	3.7 m	659 m^3	392 m^2

where $\boldsymbol{M} = \boldsymbol{M}_{\boldsymbol{RB}} + \boldsymbol{M}_{\boldsymbol{A}}$, $\boldsymbol{C} = \boldsymbol{C}_{\boldsymbol{RB}} + \boldsymbol{C}_{\boldsymbol{A}}$, and $\boldsymbol{D}$ have the same form as the bulk carrier given in Section 3.1.1. Due to limited data on the tugboat, the implemented model was based on the vessels in Table 2. While a naval vessel has large hull differences compared to a tugboat, the hydrodynamic coefficients of the naval vessel were used to find the added mass inertial matrix $\boldsymbol{M}_{\boldsymbol{A}}$. This was done since the hydrodynamic coefficients for the escort tugboat model were dimensionless [22], and to reuse the implementation method of the bulk carrier for simplicity, values of the naval vessel were chosen. The full scale data of a tugboat model was used to find more realistic values for the tugboat displacement and wetted surface area, which was used to calculate the inertial matrix $\boldsymbol{M}_{\boldsymbol{RB}}$ and nonlinear damping in surge.

The draft of the tugboat was approximated from Fig. 6, by measuring the distance from the waterline in certain points and interpolating between them. This gave the resulting draft in Fig. 7, where the hull and keel are separated to calculate the tugboat displacement from the hull draft, and cross-flow drag from both. While the azimuth thrusters would have affected both displacement and cross-flow drag, they were neglected to simplify the implementation.

Rigid body matrices. The rigid body matrices $\boldsymbol{M}_{\boldsymbol{RB}}$ and $\boldsymbol{C}_{\boldsymbol{RB}}$ in (23) were found from the mass m, the vector from CO to CG in surge direction x_g and the moment of inertia I_z. The mass was calculated from the displaced volume by combining the cross section areas along the tugboat hull with the trapezoidal rule. Each section on the tugboat was assumed to have form of a half ellipse, with breadth of the tug $B = 11.5$ m and height from the draft in Fig. 7. The calculated displacement was reduced by 10%, resulting in mass $m = 790$ tonnes. To simplify the calculations, we assume that $CG = CO \Rightarrow x_g = 0$, and moment of inertia was calculated from that of a plate, and reduced by 40% by assuming that most weight is caused by the engines close to CO, giving $I_z = 4.96 \cdot 10^7$ kgm^2.

Hydrodynamic matrices. The hydrodynamic matrices $\boldsymbol{M}_{\boldsymbol{A}}$ and $\boldsymbol{C}_{\boldsymbol{A}}$ in (24) were found based on the hydrodynamic coefficients of the naval vessel given in Table 3. Since the tugboat has a wider and larger front area, the added mass in surge $X_{\dot{u}}$ was increased. For

Table 3
Hydrodynamic coefficients for the naval vessel in Table 2, obtained from the MSS toolbox [20], and the used coefficients for Bulldog.

Vessel	$X_{\dot{u}}$	$Y_{\dot{v}}$	$Y_{\dot{r}}$	$N_{\dot{v}}$	$N_{\dot{r}}$
Naval	$-1.74 \cdot 10^4$	$-3.93 \cdot 10^5$	$-1.40 \cdot 10^6$	$5.38 \cdot 10^5$	$-3.87 \cdot 10^7$
Bulldog	$-8.00 \cdot 10^4$	$-3.90 \cdot 10^5$	$-1.00 \cdot 10^6$	$5.00 \cdot 10^5$	$-3.00 \cdot 10^7$

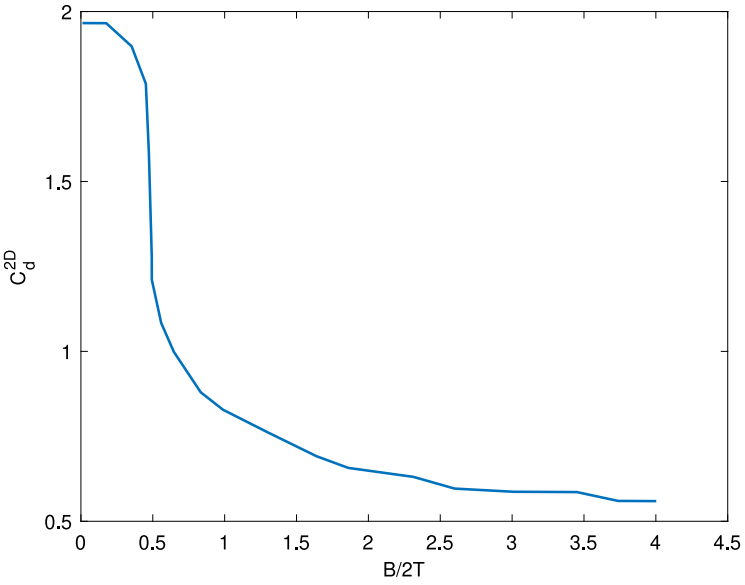

Fig. 8. Graph of the 2D cross flow coefficient C_d^{2D} as a function of the ratio between breadth and draft $B/2T$. The plot is created with data from the function "hoerner" in MSS toolbox [20].

the added mass in sway $Y_{\dot{v}}$, the values were set similarly, by assuming that the side area was around the same size, while the added mass in yaw $N_{\dot{r}}$ was lowered, as the tugboat is shorter. The cross-terms $Y_{\dot{r}}$ and $N_{\dot{v}}$ were set with the same sign and lowered, by assuming that added mass would have less impact on the stern of the hull, where acceleration in sway would cause some rotation. This resulted in a non-symmetric inertial matrix $\boldsymbol{M}$, which is positive definite if the symmetric part $\boldsymbol{M}_s = 1/2(\boldsymbol{M} + \boldsymbol{M}^\top)$ is positive definite, which can be shown from positive eigenvalues. Based on the symmetric part, the inertia matrix is positive definite. Similar to the linear damping $\boldsymbol{D}$ of the bulk carrier in (25), the linear damping for the tugboat was calculated from (10), with the time constants $T_1 = 50$, $T_2 = 80$ and $T_3 = 10$.

Nonlinear damping. To use the nonlinear damping in the tugboat dynamics $\boldsymbol{d}(\boldsymbol{\nu})$ (see (26)), the sign in the functions for nonlinear surge damping and cross-flow drag given in Section 2.1.3 was changed. From (11), the nonlinear surge damping was calculated with the wetted surface area S, a viscous correction factor $k = 0.25$ and a friction coefficient $C_f(u_r)$. The friction coefficient was adjusted to a max speed of 13 knots [21]. The wetted surface area was calculated from a box with breadth $B = 11.5$ m, length $L = 33.5$ m, and draft T (Fig. 7), and reduced by a factor of 25% resulting in $S = 672$ m^2.

The cross-flow drag was calculated from the strip theory approach in (12) and (13). At each strip, the draft from Fig. 7 was used, while the 2D drag coefficient C_d^{2D} was found with the function "hoerner" in the MSS toolbox, by using the breadth $B = 11.5$. The relation between breadth and draft for the coefficient is shown in Fig. 8, where C_d^{2D} was set to 0.5 when $B/2T > 4$.

3.2. Implementing interaction forces

3.2.1. Implementing contact force

The contact force was simulated between the tugboat bow and bulk carrier hull. To model the contacting surfaces, the hull of the bulk carrier was modelled as two straight lines, while the bow of the tugboat was assumed to have a half circular shape. The contacting point on the tug C_T and bulk carrier C_B was found by using the starboard pointing vector y_b in the bulk carrier reference frame. This gave the point closest to the hull that would make contact first (see Fig. 9).

The normal force F_N was calculated with the dissipative contact force model in (21), based on the overlapping of the contacting points (illustrated in Fig. 10), such that

$$F_N = K_N(C_B - C_T) + D_N(\dot{C}_B - \dot{C}_T)\,. \tag{27}$$

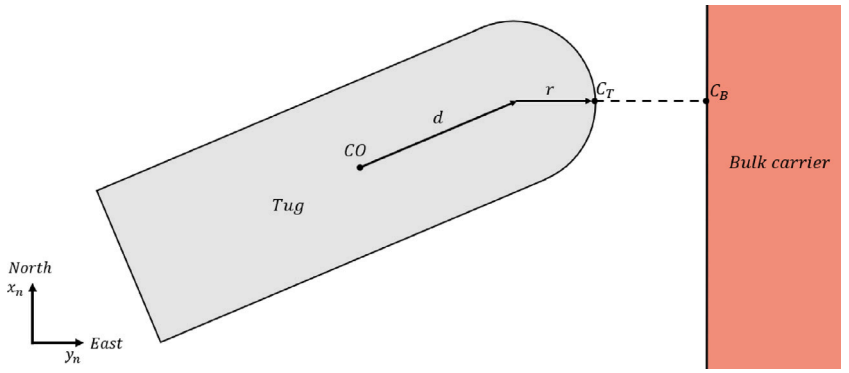

Fig. 9. The contacting points on the bulk carrier hull C_B and the tugboat fender C_T, which is on a half circle with radius $r = 5.75$ m with centre at a distance $d = 11.75$ m from the CO.

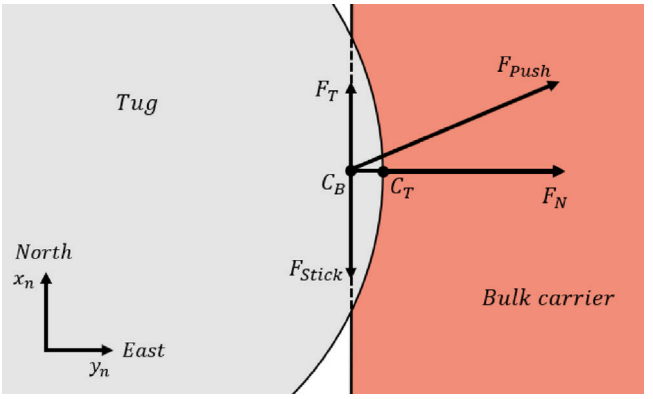

Fig. 10. Illustrating the contacting forces on the bulk carrier (moving in north direction) from the tugboat, where the direction of F_{Push} is the tugboat heading. F_{Stick} is the force required to stick the tugboat to the hull, while F_T is the tangential pushing force.

The stiffness parameter K_N was curve fitted to give the reaction force of the M600-fender from the manufacturer [23], by assuming that the contact point was one metre of fender. The damping coefficient was set to $D_N = \mu_0\sqrt{4mK_N}$, based on contact damping from Abaqus [24], with tugboat mass m and a critical damping fraction μ_0 assumed to be 0.1.

3.2.2. Implementing friction force

The friction force was used to counteract two forces between the tugboat and bulk carrier (see Fig. 10). First, the tangential force F_T in the contact point on the bulk carrier, caused by the tugboat pushing force. Second, the force required to stick the tugboat contacting point C_T at the bulk carrier hull F_{Stick}. For the tugboat to stick to the bulk carrier, the tugboat contact point C_T must have the same velocity and direction as the surge velocity of the bulk contact point C_B. Since the tugboat is seen as a rigid body, this means that the tugboat must follow in the same direction, without rotation. By using the manoeuvring model of the tugboat dynamics given in (26), the force F_{Stick} was found with the force required to move the tugboat with the contact point velocity and direction. In the manoeuvring model, the velocity and acceleration were found based on the velocity of the contact points as

$$\boldsymbol{\nu} = \boldsymbol{R}_T^\top \boldsymbol{R}_B \begin{bmatrix} \dot{C}_B & 0 & 0 \end{bmatrix}^\top \qquad \dot{\boldsymbol{\nu}} = \boldsymbol{R}_T^\top \boldsymbol{R}_B \begin{bmatrix} (\dot{C}_B - \dot{C}_T)/dt & 0 & 0 \end{bmatrix}^\top \tag{28}$$

where $\boldsymbol{R}_i, i = B, R$ is the rotational matrix in (5) for the bulk vessel and tugboat respectively, while the acceleration was calculated with a small time duration dt to give the large force required to stick instantly. This method was based on the contact model used in the boarding control system on offshore wind turbines [25], where the contact friction is modelled as a spring–damper system to capture the elasticity of the rubber fender, which uses a small mass to represent the contact point under sliding.

The total force between the vessels is then found as $F_{Tot} = F_{Stick} - F_T$, and the tugboat will stick to the bulk carrier if the force is lower than the friction force. The friction between the tugboat and the bulk carrier was simulated based on the Coulomb friction law given in (22), with both static and kinetic friction coefficients. To have a smooth transition between static friction when still and kinetic friction when the tugboat started to slide along the bulk carrier hull, an exponential term was added to the equation. This exponential transition between coefficients is also used in the Abaqus simulation program. The resulting friction force is then

$$F_R = \left((\mu_s - \mu_k)e^{-K_{v_r} v_r} + \mu_k\right) \cdot F_N \tag{29}$$

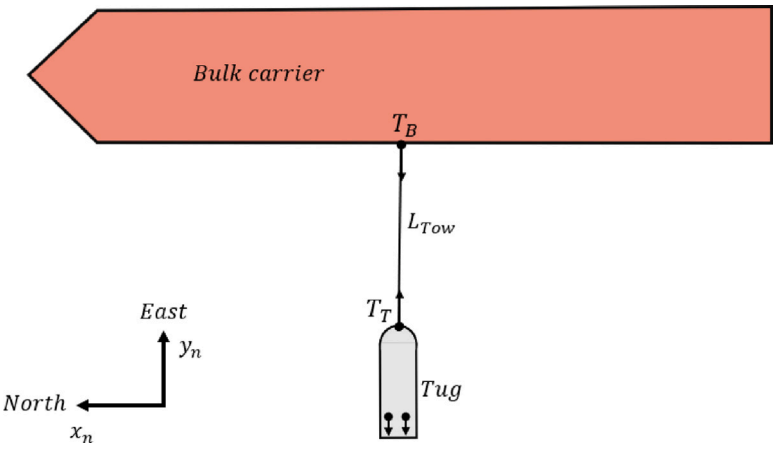

Fig. 11. Illustration of the towing operation with connection point on tug T_T and bulk carrier T_B.

where v_r is the relative velocity between the contacting points C_T and C_B in the direction along the bulk carrier hull, and K_{v_r} is a constant. The friction coefficients were based on the kinetic friction coefficient between rubber and wet asphalt,[3] between $\mu_k = 0.25 - 0.75$, to simulate a wet hull. For a relatively low stick and slip limit, the kinetic and static friction coefficients were set to $\mu_k = 0.25$ and $\mu_s = 0.4$.

The direction of the friction force was decided based on the direction of the total force F_{Tot}, where the resulting friction force on the tugboat is

$$F_R = \begin{cases} F_{Tot} & \text{if } |F_{Tot}| \leq F_R \\ F_R \cdot \text{sign}(F_{Tot}) & \text{else} \end{cases} \tag{30}$$

while the friction force on the bulk carrier is in the opposite direction. Based on the condition, the vessels will stick together when $|F_{Tot}| \leq F_R$, and slide when $|F_{Tot}| > F_R$.

3.2.3. Implementing towline force

In our model, the towline is assumed to be connected in a horizontal plane, so the increased towline force caused by the height difference between the bulk carrier and tugboat is not accounted for in the simulations. Instead, the towline is set relatively long, with a minimum of 60 m, and the force is assumed to have a small increase and therefore neglected. By having a longer towline, the impact of the propeller wash is also reduced, as seen in (19). The effect of the propeller wash is not included in the simulations, but the tugboats are kept relatively far from the hull to reduce the effects. Fig. 11 illustrates the towing operation, with a connection point on the bulk carrier T_B that could be placed along the length on either side, and the connection point on the tugboat T_T that was set to the bow centre. The towline was chosen based on the minimum requirements

$$F_{\text{min}} = K_{Tow} T_b, \qquad K_{Tow} = 2.625 - \frac{T_b}{1600} \tag{31}$$

where K_{Tow} is a safety factor based on the designed bollard pull T_b [26]. From the tugboat specifications given in [21], the designed bollard pull is 653 kN, which requires a towline that can handle a minimum of 1447 kN. Based on specifications on one type of fibre ropes used as main towlines [27], this requires a towline with diameter 48 mm, which has weight of 1.37 kg/m and minimum breaking load (MBL) of 1620 kN. Due to the relatively low weight of the towline and assuming high towline tension in operations, the stiffness of the towline only consisted of the stiffness due to elastic elongation k_E from (20). The implemented towline was assumed to be used and had a linear elongation depending on the force, with 2% elongation at MBL. Based on this, the stiffness was calculated from Hooke's law (*cf.* [19]), with $\Delta L = 0.02$ m and $F = 1620$ kN, such that

$$F = K_E \Delta L \rightarrow K_E = \frac{F}{\Delta L} = 6.63 \cdot 10^7 \text{ kN/m}. \tag{32}$$

To implement internal friction of the towline, the towline force was modelled with a dissipative damping term similar to the fender contact force in Section 3.2.1, but with a lower critical damping fraction μ_0, such that

$$F_{Tow} = K_E(T_T - T_B) + \mu_0 \sqrt{4mK_E} \cdot (\dot{T}_T - \dot{T}_B). \tag{33}$$

[3] The engineering toolbox: https://www.engineeringtoolbox.com/friction-coefficients-d_778.html.

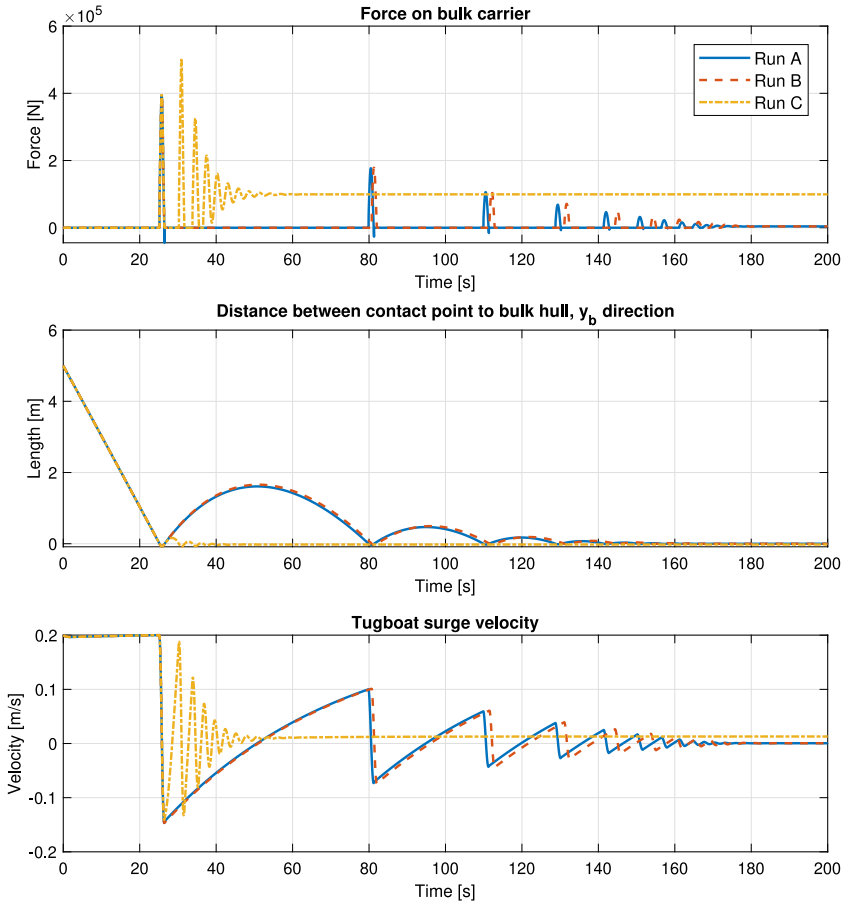

Fig. 12. Simulation results of the impact force on the bulk carrier. Run A has a constant force of 4 kN, Run B use if $F_N < 0 \Rightarrow F_N = 0$ and Run C set a desired force of 100 kN after the first contact.

4. Simulation of interaction forces

In this section, we provide simulation results of the interaction forces, which is considered the main scope of the paper. Results were created with Simulink, using an ode3 solver with fixed step size of 0.025, and show the interaction effect between a tugboat and bulk carrier generated from the contact and towing forces from Section 3. The simulator is built as a complete model setup, encompassing tugboat and vessel dynamics, interaction forces as well as guidance and control algorithms, and control allocation methods as shown in Fig. 5. The simulator is therefore a suitable and complete tool for implementing and testing control algorithms, and built on known dynamical models that have proven very advantageous for linear and nonlinear control design (*cf.* [1]). This does however increase the complexity and computational efficiency of the simulator. The simulations shown in this paper are performed for a time span of 200 s, completed within two minutes on a standard computer setup. A complete docking operation typically extends to a duration of around one hour, which we are able to simulate in 30 min. No efforts have been made at this time to optimise computational efficiency, but this is a topic for further development of the simulator.

4.1. Impact force simulations

The impact force and settling time of the contact force was simulated over three runs, with the tugboat approaching the bulk hull with a constant velocity of 0.2 m/s, from a distance of 5 m. From the results in Fig. 12, the damping term causes an undesired effect which can be seen from Run A, where there is a negative force on the bulk carrier when the tugboat moves away from the hull. This effect is removed with an "if" statement on the normal force F_N as seen with Run B, and has a small effect on the settling time. By increasing the force when contact is achieved, as seen with Run C, the force settles faster.

Impact forces can be difficult to simulate as they are sudden and often very large. In this model, the force depends on the overlapping distance and velocities, where the force could vary depending on when the first overlapping between contact surfaces is registered. The simulation results should be more consistent by using a smaller time step, but will result in longer computational time. While a time step of 0.025 s is small, the overlapping distance have a relatively large effect due to the high stiffness of the

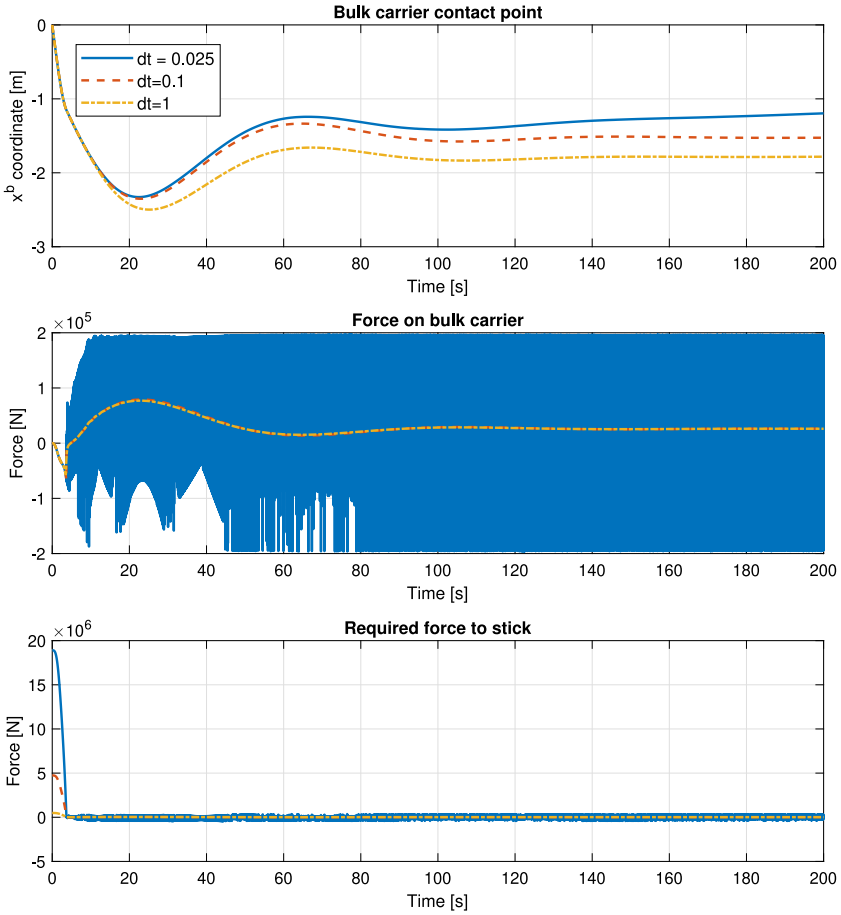

Fig. 13. Simulating contact friction with different period duration dt to calculate the acceleration based on the relative velocity between contact points (see (28)).

contacting fender. The negative force around the zero overlapping, on the return of the impact, shows that the implementation method is not accurate around the crossing. The accuracy of the model depends on the parameters used, and without real data, the actual response is difficult to simulate. While it is difficult to assume how it should be without experimental test results, high contact forces could also cause deformation on the hull and would increase the dissipative damping forces. While this may not be necessary to model, it should be considered to prevent damage on the vessels in a real system.

4.2. Friction force simulations

To simulate the friction forces between the vessels, the tugboat was assumed starting in contact facing directly at the bulk carrier hull with a desired push force, while the bulk carrier had a constant velocity around 0.4 m/s heading north.

4.2.1. Period duration simulations

To see how the period duration dt to calculate the acceleration for the tugboat stick force F_{Stick} affected the behaviour, the tugboat was simulated with a desired force of 500 kN. The results are shown in Fig. 13, where $dt = 0.025$ gives an unstable behaviour that can be seen from the fluctuations on the bulk carrier force. By increasing the time duration to $dt = 0.1$ or $dt = 1$, the force is more stable, but the initial force required to stick the tugboat to the hull is much lower. From the position of the bulk contact point, it seems like the lowest time duration $dt = 0.025$ drifts more after settling, compared to the other two.

While the acceleration of the rigid contact point should be instant to give the required stick force, there are some computational limitations. This is best seen from the unstable results with $dt = 0.025$, where the forces fluctuate. This unstable behaviour could be caused by how the vessels move compared to each other, where if one moves before the other in the simulations, a small change in velocity will generate a large force. By using a higher period duration, the initial force is reduced, but if this force is much larger than the friction force, the resulting force between the vessels should be similar. If there are large contact forces, due to pushing force or impact force, there may be larger differences. With a time duration $dt = 0.1$, the required force to stick gets relatively large,

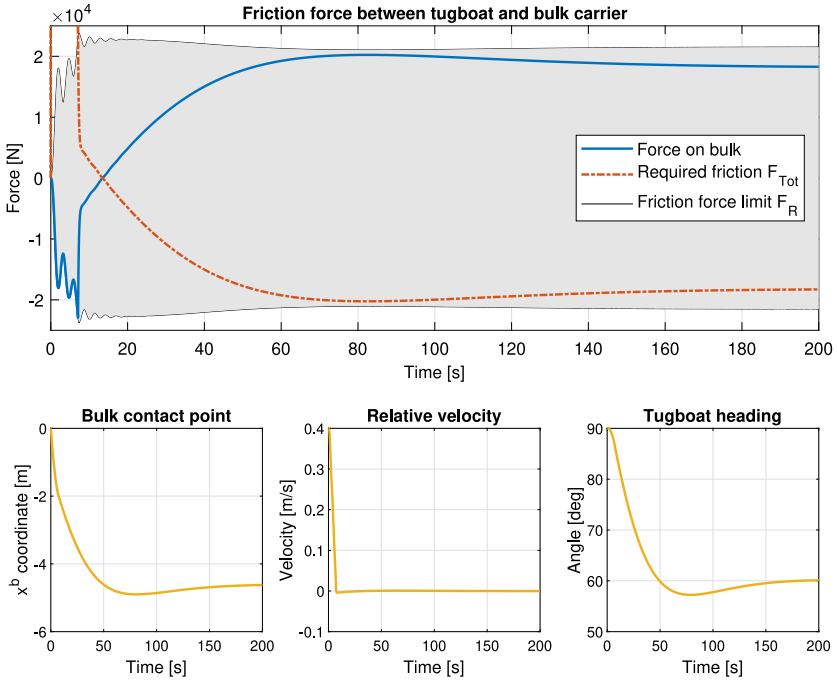

Fig. 14. Friction force simulation results of the tugboat sticking to the bulk carrier hull. The relative velocity is along the hull between contacting points.

which should be enough for a more realistic behaviour, as the rubber fender is flexible were the contact point would have a small change to accelerate.

4.2.2. Stick–slip dynamic simulations

The stick dynamics was simulated by using a desired tugboat force of 60 kN, and the results are shown in Fig. 14. First, the tugboat slide along the hull since the required stick friction F_{Tot} is larger than the friction limit F_R, which is due to the jump in relative velocity. At around 8 s, the tugboat bow stick to the hull, where the change in bulk contact point should be caused by the tugboat bow rolling along the hull, which can be seen by comparing the contact point and the tugboat heading. When the tugboat heading changes in the direction of the motion, the required friction force changes. The required friction gets close to the friction force limit, where the tugboat is close to slipping at around 80 s, before settling at an angle of around 60°. After stabilising, there is a slow drift in contact position.

A lower desired tugboat force of 40 kN was used to show the slip dynamics of the friction force, where the simulation results are shown in Fig. 15. The slip dynamics simulation is similar to the previous stick dynamics, up until about 70 s, where the tugboat starts to slide along the hull of the bulk carrier. By using a lower pushing force, the friction force limit is lower, which is enough for the required friction force to surpass the limit. When the limit is reached, the limit reduces until the relative velocity and heading starts to stabilise.

By using the tugboat dynamics to find the required friction force to stick against the hull of the bulk carrier, the transition between stick and slip seemed to be smooth. The fast decrease in the friction force limit when slipping is due to the exponential change between static and kinetic friction coefficient, which changes fast when there is motion, combined with the increasingly reduction of the contact force based on the heading.

The heading angle that the tugboat stabilises on, is explained by how the required friction force is found. Since the required friction force is based on the velocity and direction the tugboat moves through the water, the stabilising angle should be at the point when the propulsion thrust force generates a moment about the contact point equivalent to the required friction force. The heading would therefore move towards a surge direction, which has less resistance than sway direction, and stabilise if the resulting contact force is high enough.

The drift from the stick dynamics is small and would be 10–20 cm in the next 800 s, if the simulations kept going. The reason for the drift is unknown, as it could be the simplification of not using yaw rate or yaw acceleration in the calculations, or if it is due to the simulation method. While the drifting could increase depending on the velocity and desired force, the small drift should have little to no impact, as it can be compared to around 1-2° roll of the tugboat bow.

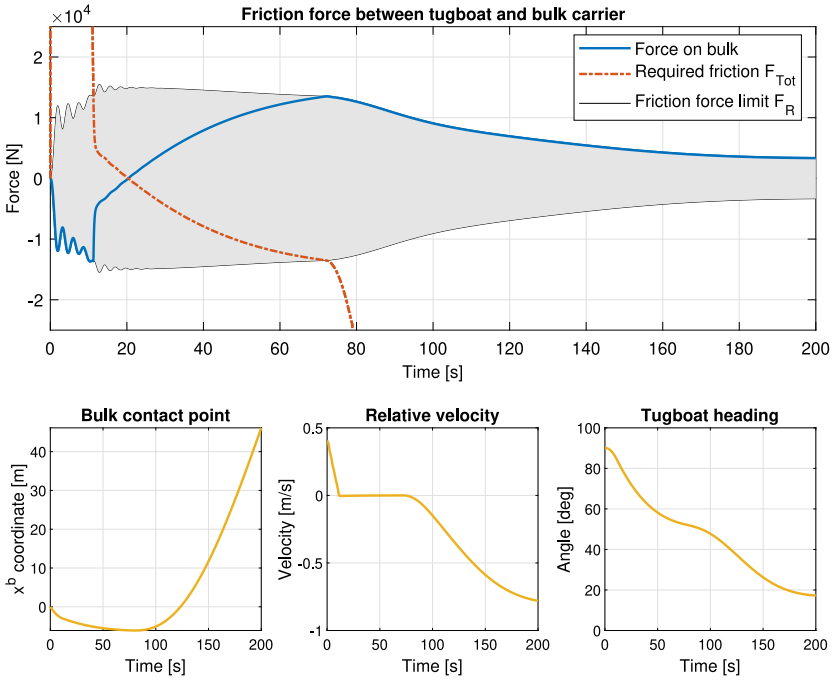

Fig. 15. Friction force simulation results of the tugboat sliding along the bulk carrier hull. The relative velocity is along the hull between contacting points.

4.3. Towline tension simulations

To simulate the forces generated by the towline tension, the tugboat started still at the towline length of 60 m from the bulk carrier, amidship (see Fig. 11), and had a desired force of −100 kN. From the simulation results shown in Fig. 16, the towline force on the bulk carrier oscillates around the desired pulling force. Without the internal friction of the towline, when the critical damping fraction $\mu_0 = 0$, the damping is only caused by the damping in the tugboat dynamics. By using a relatively low damping term, with $\mu_0 = 0.001$ and $\mu_0 = 0.01$, the oscillations settle quicker and have little impact on the total force given to the bulk carrier, which can be seen by the change in east position.

The dissipative damping term used to simulate the internal friction in the towline may be much larger than in a real towline, but removing oscillations has little impact on the change in bulk position. A higher damping term could therefore be more favourable in the simulations. While the total force on the bulk carrier is similar, the change should have a larger difference when the towline stretches with tugboat velocity. The effect should be similar as shown for the impact force in Fig. 12. For a more accurate model, the stiffness due to catenary geometry should have been implemented, which could reduce the velocity before a sudden stretching of the towline. Since the catenary stiffness depend on the towline weight, and the towline is relatively light, this effect may be to small for a short towline to make a difference.

4.4. Model discussion

The simulation shows that our derived model provides a realistic representation of dynamic forces and moments on vessel and tugboats during docking operations. From the simulation results of the towline tension and impact force, the dissipative damping is difficult to model, as small changes can make large differences. While the responses would differ in a real system, there would be large impact forces and oscillations to some degree. Combined with the stick–slip dynamics of the friction force, it should provide plausible dynamics that must be considered during a real operation. This should enlighten certain problems that must be considered in the control system designs, for using tugboats as dynamical thrusters.

The bulk carrier model dynamics was developed rather crudely, but with credible dynamics that could be used to validate a control system. For the tugboat model, due to limited data on hydrodynamic forces, the linear dynamics was based on the linear hydrodynamic forces on a different hull shape and might not be accurate. Since the nonlinear damping was based on the hull shape, the nonlinear damping could give more plausible tugboat dynamics at higher velocities. The model should therefore give some limitations to the motion, while it may not be accurate, the real system should have similar limitations at different values. Accurate models would be hard to implement as they require experimental testing, which can be expensive. However, by having more accurate models, adaptive controllers in particular should have better performance when the models have less deviation from the actual dynamics.

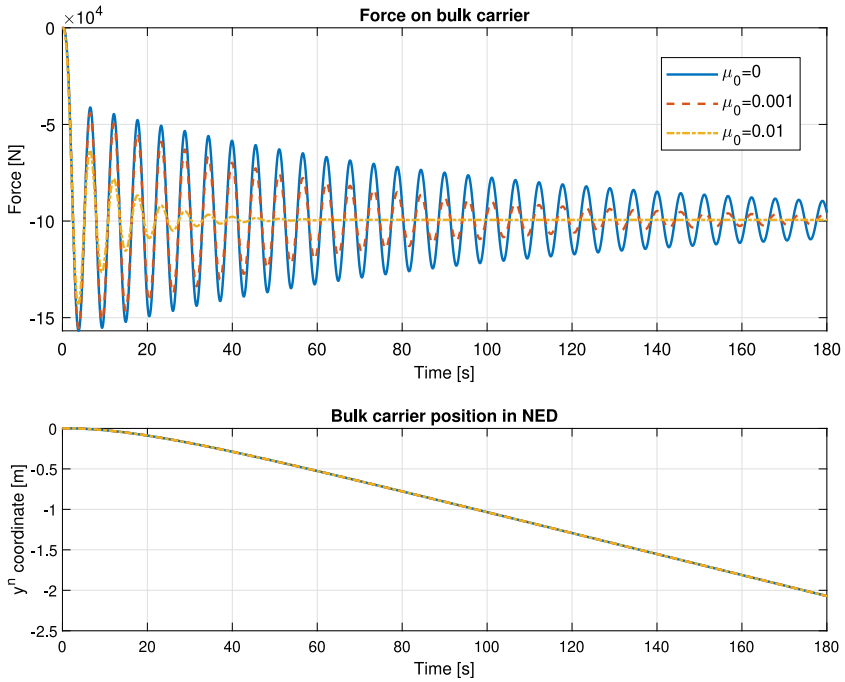

Fig. 16. Simulation results of the towline force with length 60 m modelled with different critical damping fractions μ_0 for the dissipative damping term in (33).

Since the contacting surfaces for the vessels are simplified, with straight lines for the entire bulk carrier length and a perfect circular arc for the tugboat bow, some constraints should be considered in simulations. For the bulk hull, there are certain strong sections that should be used for contact pushing, which are marked and often coincide with the towing pullerts. The strong section can be seen in Fig. 1, which lies on the midway from amidship to the bow and stern. While the tugboat bow can have a circular shape, it may have a flatter front area and narrowing sides, which should be possible to implement in a similar method. Since the tugboat sides are not modelled, the tugboat cannot make contact with the sides to follow along.

The simulation model was implemented with ideal conditions, where ocean currents, waves and wind forces are neglected. Ocean currents from the tides in Narvik and wind could have significant impact on the behaviour of the vessels, while the waves should be relatively small in harbour and have less effect. In addition, hydrodynamic interaction forces could also result in undesired motion of the vessels. One is the interaction forces caused by the tugboat propulsion system, propeller wash and the Coanda effect, where these combined can cause motion in the opposite direction of the desired force. While the propeller wash can be included in the required bollard pull, as an efficiency factor based on the towline length and projected area, the angle of the propeller wash relative to the bulk carrier hull should affect the projected area and may be challenging to model. Another is transverse thrust, which can move the stern if the towed bulk carrier is to use its own propulsion. Since the transverse thrust could change the direction in shallow waters, the force could also be challenging to model. There could also be other hydrodynamic forces that may have a significant impact on the vessels, which should require more investigation and experience from the harbour to know about.

5. Conclusion and further work

In this paper, we have presented our initial work in developing a simulator tool for tugboat-assisted docking of large vessels. Within the scope of the paper, we have developed necessary mathematical models for both tugboats and docking vessel, with a special focus on the interaction forces in pushing/pulling operations. This includes towline tension forces, contact and friction forces including stick–slip dynamics, as well as some considerations on time delay when switching between pushing and pulling operations. Implementation of the models in a Simulink simulator tool has been presented for a special case of docking of iron ore vessels in the Narvik harbour. The simulator is presented as a first step towards a more encompassing simulator system for aiding control design in autonomous docking operations, and shows realistic response and performance. For future development, we intend to investigate how we can include dissipative damping forces for more realistic interaction forces, update constraints to represent variations of tugboat bow shapes, and implement models of ocean currents and wind forces for a real world scenario. Finally, we aim to validate the simulator output through comparison of data from docking operations at the Narvik harbour.

CRediT authorship contribution statement

Raymond Kristiansen: Conceptualization, Investigation, Methodology, Project administration, Software, Supervision, Validation, Writing – original draft, Writing – review & editing. **Henning Levik Ørke:** Conceptualization, Formal analysis, Investigation,

Methodology, Software, Validation, Visualization, Writing – original draft, Writing – review & editing. **Jan Tommy Gravdahl:** Conceptualization, Formal analysis, Methodology, Supervision, Writing – review & editing.

Data availability

The simulator code is available from GitHub at https://github.com/raykris/Autodock.

References

[1] T.I. Fossen, Handbook of Marine Craft Hydrodynamics and Motion Control, second ed., Wiley, Hoboken, NJ, 2021.
[2] C. Rees, A Master's Guide to Berthing, Technical Report, Standard Club, 2021.
[3] J.M. Esposito, M. Feemster, E. Smith, Cooperative manipulation on the water using a swarm of autonomous tugboats, in: Proceedings of the IEEE International Conference on Robotics and Automation, Pasadena, CA, 2008.
[4] V.P. Bui, H. Kawai, Y.B. Kim, K.S. Lee, A ship berthing system design with four tugboats, J. Mech. Sci. Technol. 25 (2011) 1257–1264.
[5] V.P. Bui, S.W. Ji, K.H. Choi, Y.B. Kim, Nonlinear observer and sliding mode control design for dynamic positioning of a surface vessel, in: Proceedings of the International Conference on Control, Automation and Systems, Jeju Island, Korea, 2012.
[6] L. Chen, H. Hopman, R.R. Negenborn, Distributed Model Predictive Control for cooperative floating object transport with multi-vessel systems, Ocean Eng. 191 (2019) 1–16.
[7] A. Witkowska, R. Śmierzchalski, Adaptive dynamic control allocation for dynamic positioning of marine vessel based on backstepping method and sequential quadratic programming, Ocean Eng. 163 (2018) 570–582.
[8] F. Arditti, H. Cozijn, E.F.G. van Daalen, E.A. Tannuri, Dynamic positioning simulations of a thrust allocation algorithm considering hydrodynamic interactions, IFAC-PapersOnLine 51 (2018) 122–127.
[9] Z. Du, R.R. Negenborn, V. Reppa, Review of floating object manipulation by autonomous multi-vessel systems, Annu. Rev. Control 55 (2023) 255–278.
[10] H.L. Ørke, R. Kristiansen, J.T. Gravdahl, Autodock - a Simulator for Automated Tugboat-Assisted Docking of Large Vessels, Github repository, 2023, URL: https://github.com/raykris/Autodock.
[11] O. Egeland, J.T. Gravdahl, Modeling and Simulation for Automatic Control, Marine Cybernetics, Trondheim, Norway, 2002.
[12] T.A. Johansen, T.I. Fossen, Control allocation - a survey, Automatica 49 (2013) 1087–1103.
[13] H. Hensen, M. van der Laan, Towline Friction and Its Consequences, IMC Maritime System Development, 2017, Online.
[14] J. Nicholson, R. Erskine, Guidance on the Use of Tugs for Ship Assist in the Port of Southampton, Technical Report, Associated British Ports, 2021.
[15] DNV, Sea Transport Operations, Technical Report DNV-OS-H202, Det Norske Veritas, 2015.
[16] DNV, Modelling and Analysis of Marine Operation, Technical Report DNV-RP-H103, Det Norske Veritas, 2011.
[17] B.S. Massey, Mechanics of Fluids, sixth ed., Chapman & Hall, 1989.
[18] P. Flores, Contact Force Models for Multibody Dynamics, first ed., in: Solid Mechanics and Its Applications, vol. 226, Springer International Publishing, 2016.
[19] M.M. Sternheim, J.W. Kane, General Physics, second ed., John Wiley & Sons, 1991.
[20] T.I. Fossen, T. Perez, Marine Systems Simulator (MSS), 2004, URL: https://github.com/cybergalactic/MSS.
[21] BuBe, Fleet specifications - Bulldog, 2022, URL: https://www.bube.no/wp-content/uploads/2021/02/Specification_Bulldog.pdf.
[22] B. Piaggio, M. Viviani, M. Martelli, M. Figari, Z-drive escort tug manoeuvrability model and simulation, Ocean Eng. 191 (2019) 1–17.
[23] Nanjing Deers Industrial Co., Ltd, Tug boat fender, 2022, Online. URL: https://www.chinarubberfender.com/tug-boat-fender/.
[24] Abaqus, Frictional behavior, 2017, URL: https://abaqus-docs.mit.edu/2017/English/SIMACAEITNRefMap/simaitn-c-friction.htm.
[25] Ø.F. Auestad, J.T. Gravdahl, T. Perez, A.J. Sørensen, T.H. Espeland, Boarding control system for improved accessibility to offshore wind turbines: Full-scale testing, Control Eng. Pract. 45 (2015) 207–218.
[26] DNV, Rules for Classification of Ships, Technical Report DNV-RU-SHIP, Det Norske Veritas, 2021.
[27] TEHO Ropes, MAGNARO HMPE Plus rope, 2022, Online. URL: https://www.tehoropes.nl/product/magnaro-hmpe-plus-ropes/.